Andreev reflection of quantum Hall states through a quantum point contact

Mehdi Hatefipour,[1] Joseph J. Cuozzo,[2] Ido Levy,[1] William M. Strickland,[1] Dylan Langone,[1] Enrico Rossi,[3] and Javad Shabani[1,*]

[1]*Center for Quantum Information Physics, Department of Physics, New York University, New York 10003, USA*
[2]*Materials Physics Department, Sandia National Laboratories, Livermore, California 94551, USA*
[3]*Department of Physics, William & Mary, Williamsburg, Virginia 23187, USA*

(Received 20 September 2023; revised 2 December 2023; accepted 9 January 2024; published 25 January 2024)

We investigate the interplay between the quantum Hall (QH) effect and superconductivity in InAs surface quantum well (SQW)/NbTiN heterostructures using a quantum point contact (QPC). We use QPC to control the proximity of the edge states to the superconductor. By measuring the upstream and downstream resistances of the device, we investigate the efficiency of Andreev conversion at the InAs/NbTiN interface. Our experimental data is analyzed using the Landauer-Büttiker formalism, generalized to allow for Andreev reflection processes. We show that by varying the voltage of the QPC, V_{QPC}, the average Andreev reflection, A, at the QH-SC interface can be tuned from 50% to ∼10%. The evolution of A with V_{QPC} extracted from the measurements exhibits plateaus separated by regions for which A varies continuously with V_{QPC}. The presence of plateaus suggests that for some ranges of V_{QPC} the QPC might be pinching off almost completely from the QH-SC interface some of the edge modes. Our work shows an experimental setup to control and advance the understanding of the complex interplay between superconductivity and QH effect in two-dimensional gas systems.

DOI: 10.1103/PhysRevB.109.035430

I. INTRODUCTION

In recent years the realization of topological phases of matter has been a focus of intense research in the field of condensed matter physics [1–3]. This is partly motivated by the potential of such systems to host exotic quasiparticles with non-Abelian statistics, which could be used for fault-tolerant quantum computation through braiding operations [3–5]. While InAs surface quantum wells (SQWs) in proximity to superconductors have emerged as a promising platform for the realization of topological superconductivity [6–8], it is proposed that combining rich quantum Hall physics with superconductivity can allow access to higher topological states [9,10].

Recent studies [8,11–15] have demonstrated the potential of proximitizing quantum Hall edge states and superconductivity. While these studies are performed on various platforms, the signature of Andreev reflection is observed through negative downstream resistance and a reduction in Hall (upstream) resistance in the quantum Hall regime. Specifically, in Ref. [11] we showed that InAs/NbTiN systems can exhibit up to 60% Andreev conversion. This is attributed to the high efficiency of Andreev conversion at the InAs/NbTiN interface, resulting from the strong hybridization of the quantum Hall edge modes with the states in the superconductor. While cleanliness of the interface is crucial in achieving high Andreev conversion, the underlying microscopic understanding of this negative resistance is still not well understood. These recent experimental works have galvanized theoretical efforts to study Andreev processes in quantum Hall edge-state transport involving superconductivity [16–26]. In addition to the studies mentioned above, a recent study [27] has shown evidence for chiral supercurrent in quantum Hall Josephson junctions, and Ref. [28] has reported the observation of crossed Andreev reflection (CAR) across a narrow superconducting Nb electrode contacting the chiral edge state of a quantum anomalous Hall insulator (QAHI). These studies provide concrete demonstrations of the hybridization of superconductivity and quantum Hall effects.

In this work we introduce a tool frequently utilized in studying mesoscopic features of quantum Hall physics [4,29–34]: a voltage-controlled constriction known as a quantum point contact (QPC), precisely positioned on the interface between InAs and NbTiN. This placement allows us to modulate the interplay between the QH edge modes and the superconductor without altering the magnetic field or bulk filling factor of the sample. The incorporation of a QPC in our investigation serves dual purposes. Firstly, it offers precise manipulation of the interaction between edge states and the superconducting lead, facilitating control over their interaction dynamics. This unique control offers a distinct advantage by enabling a focused examination of edge-state transport while preserving intrinsic bulk properties—a feature notably absent in prior studies. Secondly, the QPC facilitates the manipulation and displacement of edge states, enabling electrical tuning towards an edge-state transport regime where the length scale of the superconducting lead (L_{sc}) becomes smaller than the edge-state length (l_e). This manipulation opens avenues for a mesoscopic-scale exploration of the interface, offering invaluable insights into the underlying transport phenomena.

II. SAMPLE GROWTH AND PREPARATION

The semiconductor in our study is a molecular beam epitaxy (MBE) heterostructure grown on a semi-insulating

*jshabani@nyu.edu

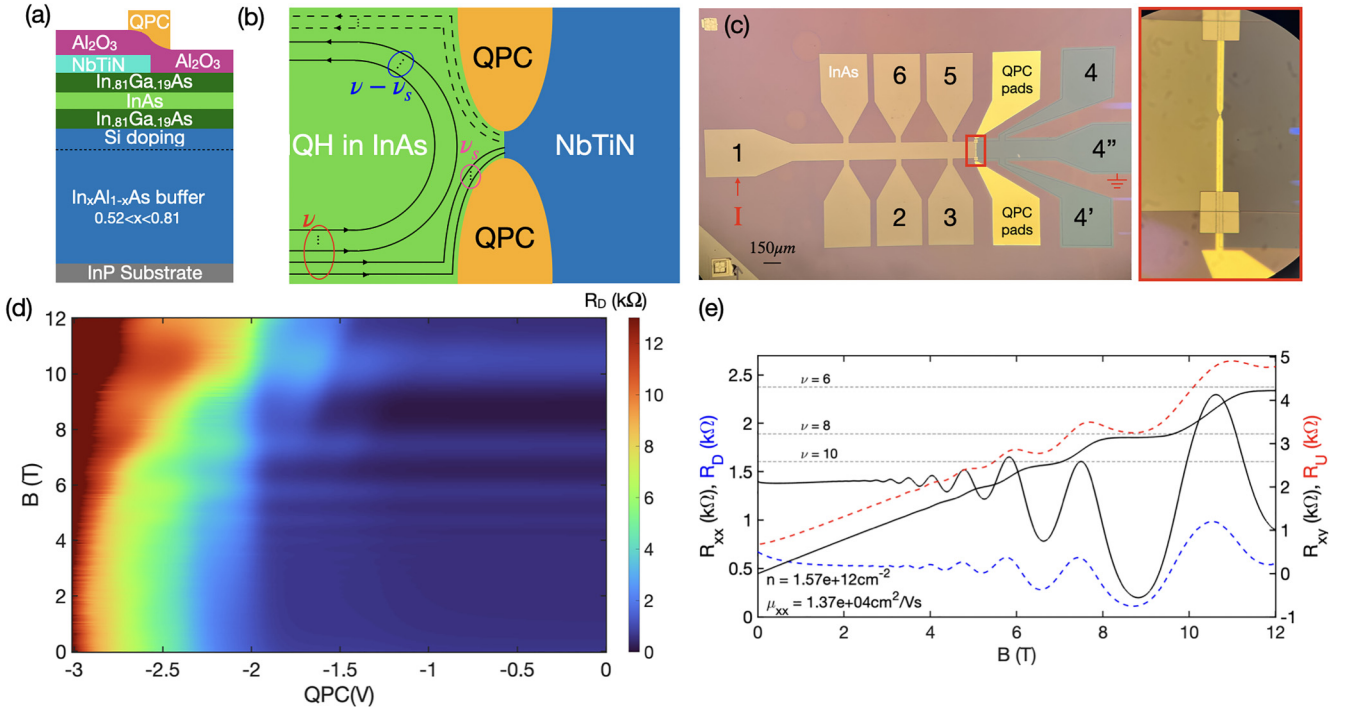

FIG. 1. (a) Schematic of the grown and fabricated layers of the sample [the region of the device specified by the red rectangle in panel (c)]. (b) Schematic diagram of the device showing the InAs/NbTiN interface with a QPC in the integer quantum Hall regime. The solid and dashed lines represent electrons and holes, respectively. When the QPC is activated, edge states allowed to pass through the QPC can be Andreev reflected off the NbTiN interface. (c) An optical photo of the finished device, highlighting the different materials labeled by color and the contacts used for current source (contact 1) and drain (contact 4″). (d) Downstream resistance (R_D) as a function of perpendicular magnetic field and QPC voltages. R_D is measured between contacts 5 and 4. (e) The 2DEG magnetotransport data of the fabricated device, where R_{xx} and R_{xy} are measured between contacts 6-5 and 5-3, respectively. The plateaus are labeled by their corresponding filling factors. Additionally, we show R_D (between contacts 5 and 4) and R_U (between 3 and 4′) plots with blue and red color, respectively.

InP(100) wafer. To form a two-dimensional electron gas (2DEG), a quantum well (QW) was grown on an $In_xAl_{1-x}As$ buffer with a graded indium content. The QW was formed by growing a 4-nm layer of $In_{0.81}Ga_{0.19}As$, a 4-nm layer of InAs, and a 10-nm layer of $In_{0.81}Ga_{0.19}As$. A δ-doped Si layer was placed below the QW at a depth of 6 nm, with a doping concentration of $n \sim 1 \times 10^{12}$ cm^{-2}. A schematic of the stack layers is shown in Fig. 1(a). These InAs quantum wells have been extensively studied in the context of mesoscopic superconductivity and topological superconducting states. Previous studies have mainly investigated the InAs/Al interface for developing tunable qubits and detecting topological superconductivity [7,35–38]. Recently the work was extended to NbTiN [11], in which the focus was the InAs/NbTiN interface in the context of semiconductor-superconductor heterostructures. In this study we aim to further explore this interface using QPCs to investigate the interplay between the integer quantum Hall effect (IQHE) and superconductivity with even greater precision.

III. DEVICE FABRICATION AND MEASUREMENT SETUP

We fabricated a Hall bar using electron-beam lithography and chemical wet etching. We cleaned the surface of the device using argon plasma etching in the sputtering tool at 25-W power for 15 s followed by deposition of a 90-nm-thick layer of NbTiN as the superconducting contacts. The interface between the InAs and NbTiN was 150 μm long, and a QPC was added with a separation of 150 nm between the QPC arms. A metallic gate for the QPC arms and pads was created by depositing 20 nm aluminum oxide (Al_2O_3) as the gate dielectric followed by 5-nm Cr and 20-nm Au e-beam deposition as the gate electrodes. Figure 1(b) shows the schematic of the device zoomed in around the QPC and interface area. The schematic demonstrates the edge mode reflection mechanism in the IQH regime and when QPC is activated. Figure 1(c) shows an optical photo of the finished device, labeling different regions by their corresponding materials. We have fabricated two samples (A and B) to confirm our observations; however, we mainly focus on sample A data in the main text and show all the data for sample B in the Supplemental Material (SM) [39]. The experiment was performed in a dilution fridge at a temperature of $T \sim 30$ mK with a maximum magnetic field of 12 T. The magnetotransport experiment was carried out using lock-in amplifiers and an AC four-point measurement technique with a frequency of <20 Hz and $I_{ac} = 1$ μA AC excitation current.

IV. MEASUREMENT RESULTS

Magnetotransport data

In order to assess the mobility of the quantum well in our fabricated device, we conducted magnetotransport

experiments on the 2DEG. As shown in Fig. 1(c), we utilized contact 1 as the current source and 4″ as the current drain, and measured R_{xx}(6-5) and R_{xy}(5-3) as a function of magnetic field for mobility and density analysis. Our measurements revealed that the mobility of the QW for sample A is approximately $\mu \sim 13\,700$ cm^2/V s at an electron density of $n = 1.54 \times 10^{12}$ cm^{-2}. This mobility value corresponds to an electron mean free path of approximately $l_e \sim 280$ nm. The data for R_{xx} and R_{xy} as a function of magnetic field is shown in Fig. 1(e), which indicates that the sample has a relatively high density. Several oscillations and plateaus in the longitudinal and Hall transport data are observed in the 12T window, respectively corresponding to filling factors $\nu = 6$, 8, and 10. Figure 1(d) displays the downstream resistance R_D (measured between contacts 5 and 4) as a function of QPC voltage and perpendicular magnetic field.

To understand the transport properties of mesoscopic systems, the Landauer-Büttiker (LB) formalism is widely used [40]. It is important to note that conventional Blonder-Tinkham-Klapwijk (BTK) analysis is inadequate for describing semiconductor-superconductor interfaces under the quantum Hall regime. In this regime, electron modes in the quantum well become nonlocalized edge modes along the semiconductor-superconductor interface, deviating from BTK assumptions. Our analysis diverges from the standard BTK treatment due to this fundamental difference, as detailed in Ref. [11] and other works [41–43]. These references offer a more suitable framework for understanding semiconductor-superconductor interfaces amidst the QH effect.

When a superconductor is present, Andreev reflection (AR) processes can occur at the interface between the semiconductor and the superconductor [44]. To include the possibility of AR, we have extended the LB formalism describing edge-state transport in a Hall bar geometry. The effect of the AR is captured by the average Andreev reflection $A \equiv (1/\nu)\sum_{i=1..\nu} A_i$, where ν is the total number of edge modes, and A_i is the probability of Andreev reflection, i.e., $A_i = T_{53}^{he}(i)$ is the transmission probability of an electron edge state in the ith band incident from lead 3 converting to a hole edge state in lead 5 [Fig. 1(c)].

The values of A_i can only be obtained microscopically as described in Refs. [11,21,26,41]. Details of the interface, transverse spatial profile of the QH edge modes, edge reconstruction, distance of edge modes from the semiconductor-superconductor interface, and spatial profile of the electronic states in the superconductor affect A_i and therefore the average A. A voltage on the QPC affects these details and so modifies A. As the voltage on the QPC is tuned to larger negative values, the distance of the QH edge modes from the superconductor increases, leading to regimes in which A decreases gradually, alternated by regimes in which some of the QH edge modes are completely pinched off from the semiconductor-superconductor interface and A drops sharply to a lower value. For this reason the LB treatment is valid also for values of $V_{\rm QPC}$ for which A is not constant, and in particular, also for values of $V_{\rm QPC}$ smaller than -2 V.

We assume the chirality of edge states is preserved. This assumption breaks down in the case where bulk conduction becomes significant. Furthermore, the Landauer-Büttiker formalism we consider here breaks down when the superconducting electrode is pinched off from the edge states by the QPC so that no current is flowing to the superconducting contact via Andreev reflection. This breakdown is evident in the divergence of the upstream and downstream resistances when $V_{\rm QPC} < -3$ V, so we will restrict our analysis to QPC voltages greater than -3 V.

Following our previous work [11], we begin by considering the six-terminal configuration shown in Fig. 1(b). The terminals 1, 2, 3, 5, and 6 are considered as ideal metallic leads, while contact 4 is a superconducting lead. Let I_i and V_i denote the currents and voltages, respectively, at the terminals $i = (1, 2, ..., 6)$. The superconducting contacts 4, 4′, and 4″ are at the same potential so that we need only consider the voltage V_4. Without loss of generality, we set $V_4 = 0$. The conservation of charge equation $\sum_i I_i = 0$ is employed to express I_4 in terms of the currents at the other leads. Using these considerations, the Landauer-Büttiker equations take the form

$$\begin{pmatrix} I_1 \\ I_2 \\ I_3 \\ I_5 \\ I_6 \end{pmatrix} = \frac{\nu}{R_H} \begin{pmatrix} 1 & 0 & 0 & 0 & -1 \\ -1 & 1 & 0 & 0 & 0 \\ 0 & -1 & 1 & 0 & 0 \\ 0 & 0 & 2A-1 & 1 & 0 \\ 0 & 0 & 0 & -1 & 1 \end{pmatrix} \begin{pmatrix} V_1 \\ V_2 \\ V_3 \\ V_5 \\ V_6 \end{pmatrix}, \tag{1}$$

where ν represents the total number of edge states R_H, the Hall resistance (h/e^2), and A the average probability of Andreev reflection per edge mode.

By assuming that no current flows into leads 2, 3, 5, and 6, we can simplify the equation by setting $I_2 = I_3 = I_5 = I_6 = 0$. We set the voltages at terminals 1, 2, and 3 equal to each other, $V_1 = V_2 = V_3$, and the voltages at terminals 5 and 6 equal to each other, $V_5 = V_6$. Let $I = I_1 = -I_4$. With these assumptions we can solve Eq. (1) to obtain

$$R_U = \frac{V_3 - V_4}{I} = \frac{R_H}{\nu}\frac{1}{2A}, \tag{2}$$

$$R_D = \frac{V_5 - V_4}{I} = \frac{R_H}{\nu}\left(\frac{1}{2A} - 1\right). \tag{3}$$

The set of equations outlined above provides a theoretical framework for studying edge-state transport in the IQH/SC hybrid system.

Starting with the case where the QPC voltage is zero, we can extract A using Eqs. (2) and (3) from R_U and R_D. In Fig. 2(a) we show the extracted A at different filling factors for sample A studied in this work. We see that for $V_{\rm QPC} = 0$ the value of A falls within the range of 40%–50% and that the extracted value of A is found to be consistent between upstream and downstream resistances. Sample B shows a similar trend at higher filling factors ($\nu = 12$, 14, 16), as shown in the SM [39].

Figure 3 shows the downstream resistance as a function of QPC voltage for different fillings ($\nu = 6$, 8, 10). In each case the downstream resistance remains constant for voltages $\gtrsim -1.5$ V before increasing. In Fig. 4 we present the upstream resistance at the same magnetic fields and QPC range as Fig. 3. There we also observe an increase in the resistance with decreasing QPC voltage for $V_{\rm QPC} < -1.5$ V. We can check

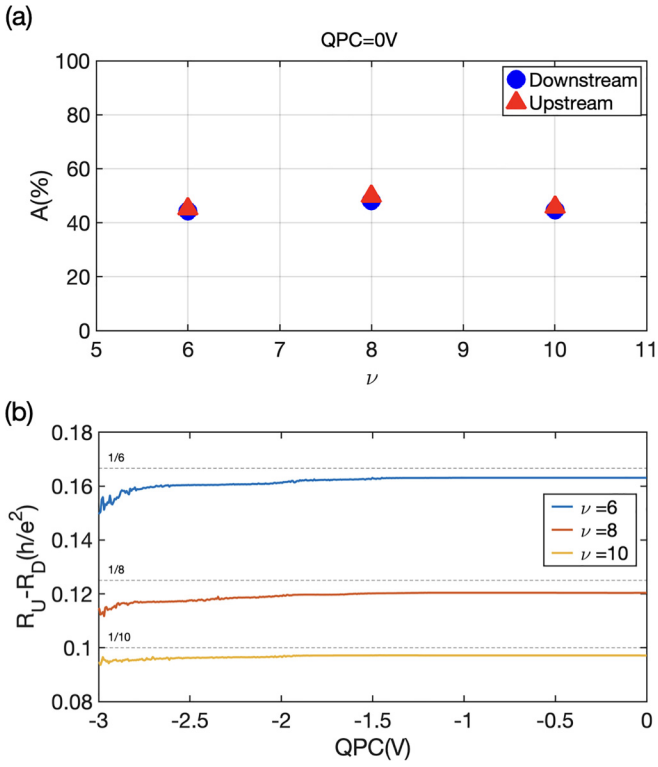

FIG. 2. (a) Extracted Andreev reflection data for three distinct filling factors: 6, 8, and 10. This data is derived from both the R_D and R_U datasets, and with a QPC voltage of 0 V. (b) Dependence of the difference $R_U - R_D$ on QPC voltage.

the consistency of Eqs. (2) and (3) with the experimental measurements by considering the difference $(R_U - R_D)$. According to Eqs. (2) and (3), $(R_U - R_D) = h/(\nu e^2)$, regardless of the transmission through the QPC. From Fig. 2(b) we see the difference in resistances remains fairly constant with QPC voltage > -3 V and corresponds to the expected filling. This suggests that Eqs. (2) and (3) consistently model the experimental data between the two edge-state transport regimes for $V_{\rm QPC} > -3$ V. We note that our initial assumption of constant $I_{\rm ac} = 1\,\mu$A is subject to real-world conditions. In reality, the presence of line imperfections and sample resistivity leads to a reduced actual current, thereby affecting the measured values in comparison to the expected quantized values (dashed lines). When the QPC voltage falls below -3 V, R_U and R_D quickly diverge and the LB model breaks down. From the experimental measurement of R_D and R_U shown in Figs. 3 and 4, using Eqs. (2) and (3), we can obtain the evolution of A with $V_{\rm QPC}$ for different filling factors ν. Figure 5 shows the obtained average Andreev conversion probability. We see that regardless of the bulk filling factor, A is suppressed by the QPC. We also observe that for $V_{\rm QPC} < -1$ V, A first decreases continuously and then, for some ranges of $V_{\rm QPC}$, exhibits plateaus, as can be seen most clearly for the case $\nu = 8$ when $-2 < V_{\rm QPC} < -1.7$ V. The continuous decrease of A with $V_{\rm QPC}$ can be interpreted as due to the progressive reduction of the superconducting pairing correlations induced by the superconductor into the QH edge modes as the QPC pushes away the edge modes from the QH-SC interface. As $V_{\rm QPC}$ reaches threshold values, some of the edge modes further

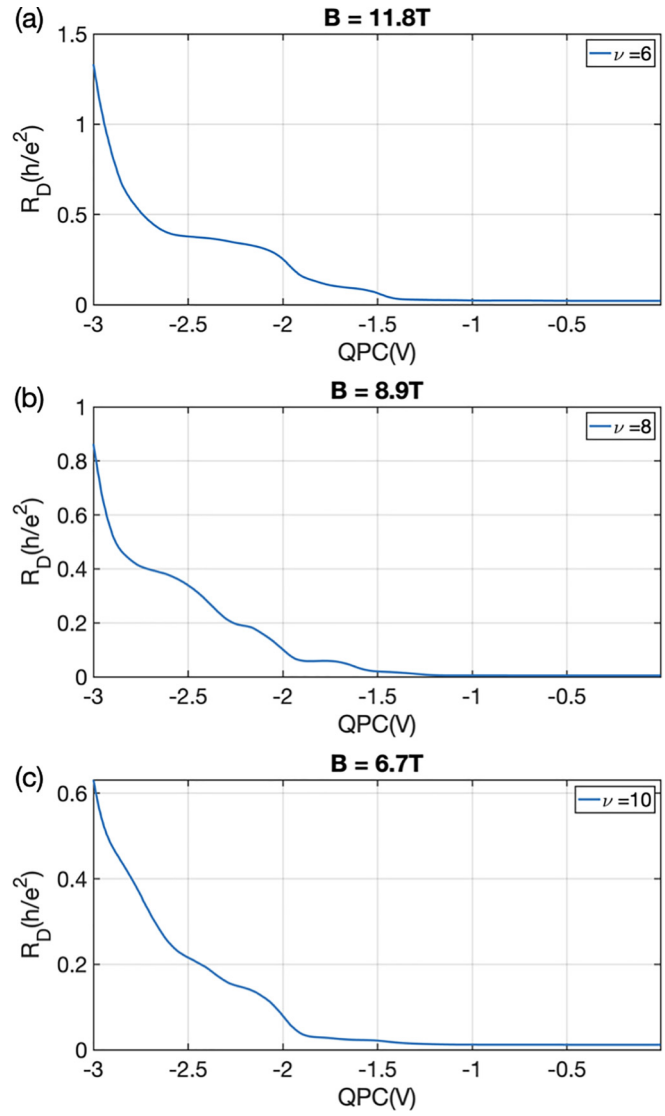

FIG. 3. Measured downstream resistance (R_D) as a function of QPC voltage for different values of ν: (a) 6, (b) 8, and (c) 10. The magnetic field for each filling factor is labeled on top of each panel.

removed from the edge are almost completely pinched off from the QH-SC interface, resulting in a new, reduced value of A that approximately is not affected by a further decrease of $V_{\rm QPC}$ until $V_{\rm QPC}$ is large enough, in absolute value, to significantly affect the pairing correlations of one more edge mode. Let the number of edge states remaining be ν_s. Then for the ranges of $V_{\rm QPC}$ for which A is approximately constant, we can assume that $\nu_s < \nu$ modes have a value of $A \neq 0$, while $\nu - \nu_s$ modes have $A \approx 0$. A discussion of the corresponding modifications to the LB model is found in the SM [39]. One of the effects of the QPC is to also reduce the effective length, L_{sc}, of the QH-SC interface. When $V_{\rm QPC} = 0$, we can assume $L_{sc} = L = 150\,\mu$m. For the largest absolute value of $V_{\rm QPC}$, L_{sc} can be taken to be equal to the distance between the two gates forming the QPC: $L_{sc} = 150$ nm.

NbTiN is a type-II superconductor with an upper critical field H_{c2} of the order of 28 T [11]. As a consequence, the coherence length ξ of NbTiN is quite small (∼5nm), and for the range of magnetic field considered, 0–12 T, can be

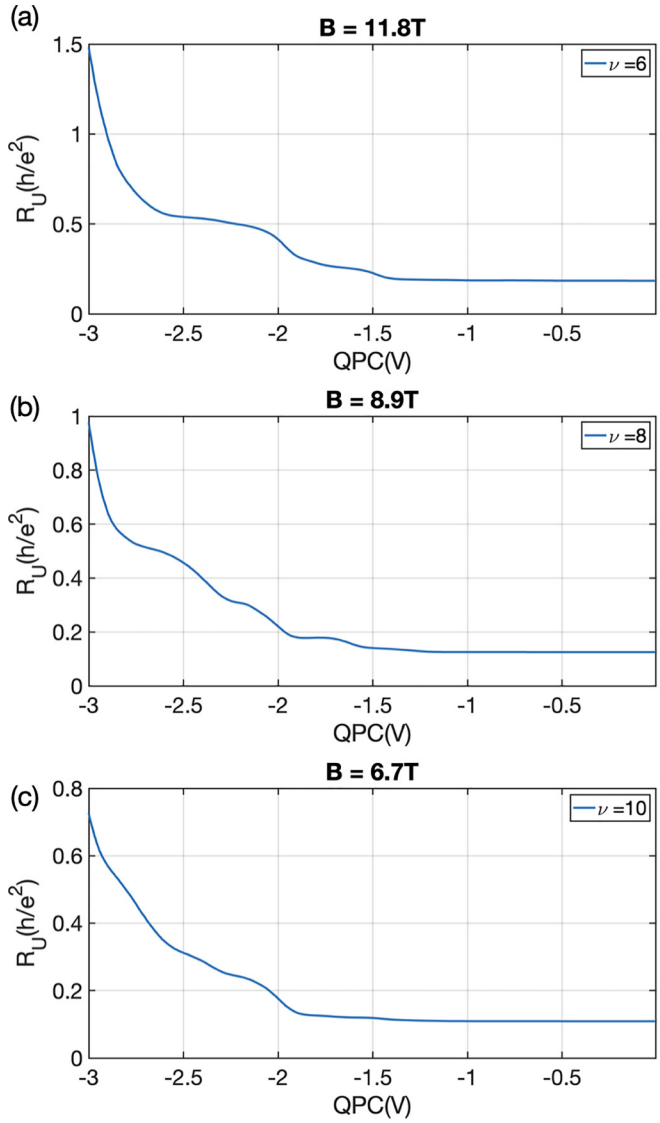

FIG. 4. Measured upstream resistance (R_U) as a function of QPC voltage for different values of ν: (a) 6, (b) 8, and (c) 10.

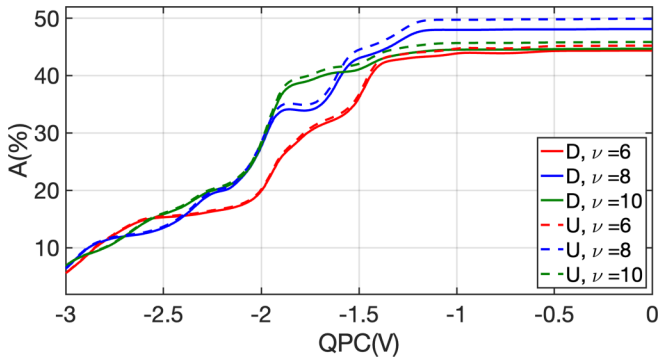

FIG. 5. The extracted A parameter from both upstream (U) and downstream (D) resistance for different filling factors ν as a function of QPC voltage.

assumed to be constant given that the largest magnetic field used is more than a factor of 2 smaller than H_{c2}. The fact that NbTiN is a type-II superconductor also guarantees that the superconducting gap is not significantly suppressed for the range of values of magnetic fields considered. Then, regardless of whether the QPC is activated or not, $\xi \ll L_{sc}$, so that crossed Andreev reflection processes can be neglected [8,12]. However, one would expect that the variation of L_{sc} induced by V_{QPC} would induce oscillations in A. The lack of oscillations of A with V_{QPC} suggests that effects due to disorder and vortices in NbTiN might play an important role, resulting in an effective averaging of A over L_{sc}, as proposed in Ref. [11], giving rise to a value of A averaged along the length L_{sc} that is independent of L_{sc} as long as L_{sc} is much large than the superconducting coherence length ξ of the superconductor.

V. CONCLUSION

Our work demonstrates the successful fabrication of a hybrid device at the InAs/NbTiN interface, incorporating a quantum point contact. We have shown that by tuning the QPC voltage, the effective, average, Andreev conversion probability A for QH edge modes can be tuned. We find that there are threshold values of the QPC voltage for which some of the QH edge modes appear to be completely pinched off by the QPC from the QH-SC interface, resulting in plateaus in the scaling of A with V_{QPC}. The results also show that the variation induced by the QPC of the effective length L_{sc} of the QH-SC interface does not result in oscillations of A. This is consistent with the findings of Ref. [11] and suggests that effects due to disorder and vortices in NbTiN must play an important role in determining the properties of chiral Andreev states in InAs/NbTiN QH-SC heterojunctions, resulting on an effective averaging of A over L_{sc} that is independent of L_{sc} as long as L_{sc} is much larger than the superconductor's coherence length. These findings advance the understanding of QH-SC interfaces and should motivate future works to further elucidate the details of the interplay of QH and superconducting states.

The DOE will provide public access to results of federally sponsored research in accordance with the DOE Public Access Plan [45].

ACKNOWLEDGMENTS

This work was supported by US DOE BES Grant No. DE-SC0022245 and U.S. Army Research Office Agreement No. W911NF1810067. The work at Sandia is supported by a LDRD project. E.R. thanks KITP, supported in part by the National Science Foundation under Grants No. NSF PHY-1748958 and No. PHY-2309135, where part of this work was performed.

Sandia National Laboratories is a multimission laboratory managed and operated by National Technology & Engineering Solutions of Sandia, LLC (NTESS), a wholly owned subsidiary of Honeywell International Inc., for the U.S. Department of Energy's National Nuclear Security Administration (DOE/NNSA) under Contract No. DE-NA0003525. Any subjective views or opinions that might be expressed in

[1] A. Y. Kitaev, Phys. Usp. **44**, 131 (2001).
[2] C. W. J. Beenakker, Annu. Rev. Condens. Matter Phys. **4**, 113 (2013).
[3] J. Alicea, Rep. Prog. Phys. **75**, 076501 (2012).
[4] C. Nayak, S. H. Simon, A. Stern, M. Freedman, and S. D. Sarma, Rev. Mod. Phys. **80**, 1083 (2008).
[5] A. Laucht, S. Simmons, R. Kalra, G. Tosi, J. P. Dehollain, J. T. Muhonen, S. Freer, F. E. Hudson, K. M. Itoh, D. N. Jamieson *et al.*, Phys. Rev. B **94**, 161302(R) (2016).
[6] M. Aghaee, A. Akkala, Z. Alam, R. Ali, A. A. Ramirez, M. Andrzejczuk, A. E. Antipov, P. Aseev, M. Astafev, B. Bauer *et al.* (Microsoft Quantum), Phys. Rev. B **107**, 245423 (2023).
[7] M. C. Dartiailh, W. Mayer, J. Yuan, K. S. Wickramasinghe, A. Matos-Abiague, I. Žutić, and J. Shabani, Phys. Rev. Lett. **126**, 036802 (2021).
[8] J. S. Lee, B. Shojaei, M. Pendharkar, A. P. McFadden, Y. Kim, H. J. Suominen, M. Kjaergaard, F. Nichele, H. Zhang, C. M. Marcus *et al.*, Nano Lett. **19**, 3083 (2019).
[9] R. S. K. Mong, D. J. Clarke, J. Alicea, N. H. Lindner, P. Fendley, C. Nayak, Y. Oreg, A. Stern, E. Berg, K. Shtengel *et al.*, Phys. Rev. X **4**, 011036 (2014).
[10] D. J. Clarke, J. Alicea, and K. Shtengel, Nat. Commun. **4**, 1348 (2013).
[11] M. Hatefipour, J. J. Cuozzo, J. Kanter, W. M. Strickland, C. R. Allemang, T.-M. Lu, E. Rossi, and J. Shabani, Nano Lett. **22**, 6173 (2022).
[12] O. Gül, Y. Ronen, S. Y. Lee, H. Shapourian, J. Zauberman, Y. H. Lee, K. Watanabe, T. Taniguchi, A. Vishwanath, A. Yacoby *et al.*, Phys. Rev. X **12**, 021057 (2022).
[13] L. Zhao, E. G. Arnault, A. Bondarev, A. Seredinski, T. F. Q. Larson, A. W. Draelos, H. Li, K. Watanabe, T. Taniguchi, F. Amet *et al.*, Nat. Phys. **16**, 862 (2020).
[14] L. Zhao, Z. Iftikhar, T. F. Q. Larson, E. G. Arnault, K. Watanabe, T. Taniguchi, F. Amet, and G. Finkelstein, Phys. Rev. Lett. **131**, 176604 (2023).
[15] F. Amet, C. T. Ke, I. V. Borzenets, J. Wang, K. Watanabe, T. Taniguchi, R. S. Deacon, M. Yamamoto, Y. Bomze, S. Tarucha *et al.*, Science **352**, 966 (2016).
[16] Y. Tang, C. Knapp, and J. Alicea, Phys. Rev. B **106**, 245411 (2022).
[17] A. David, J. S. Meyer, and M. Houzet, Phys. Rev. B **107**, 125416 (2023).
[18] V. D. Kurilovich, Z. M. Raines, and L. I. Glazman, Nat. Commun. **14**, 2237 (2023).
[19] A. B. Michelsen, P. Recher, B. Braunecker, and T. L. Schmidt, Phys. Rev. Res. **5**, 013066 (2023).
[20] V. D. Kurilovich and L. I. Glazman, Phys. Rev. X **13**, 031027 (2023).
[21] A. L. R. Manesco, I. M. Flór, C.-X. Liu, and A. R. Akhmerov, SciPost Phys. Core **5**, 045 (2022).
[22] M. Beconcini, M. Polini, and F. Taddei, Phys. Rev. B **97**, 201403(R) (2018).
[23] Y. Alavirad, J. Lee, Z.-X. Lin, and J. D. Sau, Phys. Rev. B **98**, 214504 (2018).
[24] N. Schiller, B. A. Katzir, A. Stern, E. Berg, N. H. Lindner, and Y. Oreg, Phys. Rev. B **107**, L161105 (2023).
[25] T. H. Galambos, F. Ronetti, B. Hetényi, D. Loss, and J. Klinovaja, Phys. Rev. B **106**, 075410 (2022).
[26] J. J. Cuozzo and E. Rossi, arXiv:2306.12483.
[27] H. Vignaud, D. Perconte, W. Yang, B. Kousar, E. Wagner, F. Gay, K. Watanabe, T. Taniguchi, H. Courtois, Z. Han *et al.*, Nature **624**, 545 (2023).
[28] A. Uday, G. Lippertz, K. Moors, H. F. Legg, A. Bliesener, L. M. C. Pereira, A. A. Taskin, and Y. Ando, arXiv:2307.08578.
[29] A. Bid, N. Ofek, M. Heiblum, V. Umansky, and D. Mahalu, Phys. Rev. Lett. **103**, 236802 (2009).
[30] J. Gabelli, G. Fève, T. Kontos, J.-M. Berroir, B. Placais, D. C. Glattli, B. Etienne, Y. Jin, and M. Büttiker, Phys. Rev. Lett. **98**, 166806 (2007).
[31] D. Sánchez and M. Moskalets, Entropy **22**, 977 (2020).
[32] I. Taktak, M. Kapfer, J. Nath, P. Roulleau, M. Acciai, J. Splettstoesser, I. Farrer, D. A. Ritchie, and D. C. Glattli, Nat. Commun. **13**, 5863 (2022).
[33] S. Baer, C. Rössler, T. Ihn, K. Ensslin, C. Reichl, and W. Wegscheider, Phys. Rev. B **90**, 075403 (2014).
[34] K. Zimmermann, A. Jordan, F. Gay, K. Watanabe, T. Taniguchi, Z. Han, V. Bouchiat, H. Sellier, and B. Sacépé, Nat. Commun. **8**, 14983 (2017).
[35] T. W. Larsen, K. D. Petersson, F. Kuemmeth, T. S. Jespersen, P. Krogstrup, J. Nygård, and C. M. Marcus, Phys. Rev. Lett. **115**, 127001 (2015).
[36] L. Casparis, M. R. Connolly, M. Kjaergaard, N. J. Pearson, A. Kringhøj, T. W. Larsen, F. Kuemmeth, T. Wang, C. Thomas, S. Gronin *et al.*, Nat. Nanotechnol. **13**, 915 (2018).
[37] H. Ren, F. Pientka, S. Hart, A. T. Pierce, M. Kosowsky, L. Lunczer, R. Schlereth, B. Scharf, E. M. Hankiewicz, L. W. Molenkamp *et al.*, Nature (London) **569**, 93 (2019).
[38] A. Fornieri, A. M. Whiticar, F. Setiawan, E. Portolés, A. C. C. Drachmann, A. Keselman, S. Gronin, C. Thomas, T. Wang, R. Kallaher *et al.*, Nature (London) **569**, 89 (2019).
[39] See Supplemental Material at http://link.aps.org/supplemental/10.1103/PhysRevB.109.035430 for details of a modified Landauer-Buttiker model with QPC.
[40] M. Büttiker, Phys. Rev. Lett. **57**, 1761 (1986).
[41] J. A. M. van Ostaay, A. R. Akhmerov, and C. W. J. Beenakker, Phys. Rev. B **83**, 195441 (2011).
[42] C. W. J. Beenakker, Phys. Rev. Lett. **64**, 216 (1990).
[43] J. P. Dahlhaus, J. M. Edge, J. Tworzydło, and C. W. J. Beenakker, Phys. Rev. B **84**, 115133 (2011).
[44] H. Hoppe, U. Zülicke, and G. Schön, Phys. Rev. Lett. **84**, 1804 (2000).
[45] https://energy.gov/downloads/doe-public-access-plan.

S.I. : Andreev reflection of quantum Hall states through a quantum point contact

Mehdi Hatefipour[1], Joseph J. Cuozzo[2], Ido Levy[1], William M. Strickland[1], Dylan Langone[1], Enrico Rossi[3], and Javad Shabani[1*]
[1] *Center for Quantum Information Physics , Department of Physics, New York University, NY 10003, USA*
[2] *Materials Physics Department, Sandia National Laboratories, Livermore, CA 94551, USA*
[3] *Department of Physics, William & Mary, Williamsburg, Virginia 23187, USA*
(Dated: December 2, 2023)

SAMPLE B EXPERIMENTAL ANALYSIS

In this section, we provide a comprehensive overview of the magnetotransport data obtained for sample B, following the experimental procedures detailed in the main text. Figure 1 showcases the magnetic field-dependent behavior of R_{xx} and R_{xy}. Unfortunately, during the 2DEG characterization experiment, we encountered contact failures that restricted us from reaching magnetic field strengths beyond 5.6 T. Consequently, this limitation introduced a noticeable level of out-of-phase noise into our measurements.

Moving forward, in Fig. 2, we present Andreev reflection data extracted from both the upstream (R_U) and downstream (R_D) resistance datasets for distinct filling factors (ν = 12, 14, and 16). These measurements were conducted at a QPC voltage of 0 V, allowing us to investigate the interplay between Andreev reflections and filling factors.

Figure 3 delves into the downstream resistance (R_D) as a function of QPC voltage, unveiling its behavior for the same filling factors ($\nu = 12$, 14, and 16). The magnetic field corresponding to each filling factor is annotated above the respective panel, providing context for the observed trends.

On the other hand, Fig. 4 depicts the upstream resistance (R_U) as it varies with QPC voltage across different filling factors (ν = 12, 14, and 16). This data allows us to gain insights into the behavior of the upstream resistance under varying experimental conditions.

Lastly, in Fig. 5, we explore the A parameter, which has been derived from both the upstream (U) and downstream (D) resistance datasets. This parameter is examined as a function of QPC voltage.

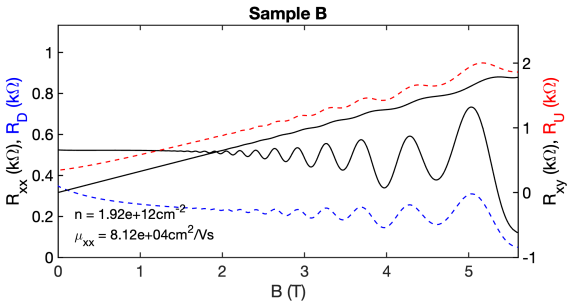

FIG. 1: The figure shows the magnetotransport data for sample B, with the R_{xx} and R_{xy} plotted as a function of magnetic field. Additionally, the density, calculated from the linear region of the Hall data, and the mobility have been indicated on the plot.We've also included R_D and R_U plots represented in blue and red colors, respectively.

MODIFIED LANDAUER-BÜTTIKER MODEL WITH QPC

In the experiment, as the QPC voltage is decreases, R_D and R_U begin to increase and exhibit plateaus which suggest a gradual pinching off of edge states reaching the NbTiN lead. In this section we incorporate a simple model of the QPC into the modified Landauer-Büttiker model discussed in Eq. (1-3) in the main text. Let ν be the bulk filling factor and ν_s be the number of edge states passing through the QPC. We define the average Andreev conversion $A = \frac{1}{\nu}\sum_i^{\nu} a_i$ where a_i is the probability of Andreev conversion in the i^{th} edge channel. To qualitatively capture the effect of the QPC, we will make the strong assumption that modes are completely pinched off abruptly with the QPC voltage. To capture this, we define an average Andreev conversion through the QPC $A_s = \frac{1}{\nu_s}\sum_i^{\nu_s} a_i$ where we eliminated a_j for $\nu_s < j \leq \nu$. Then $\nu A = \nu_s A_s$ and the modified Landauer-Büttiker model gives us

$$R_U = \frac{V_3 - V_4}{I} = \frac{R_H}{\nu_s}\frac{1}{2A_s} \tag{1}$$

$$R_D = \frac{V_5 - V_4}{I} = \frac{R_H}{\nu}\left(\frac{\nu}{2A_s\nu_s} - 1\right). \tag{2}$$

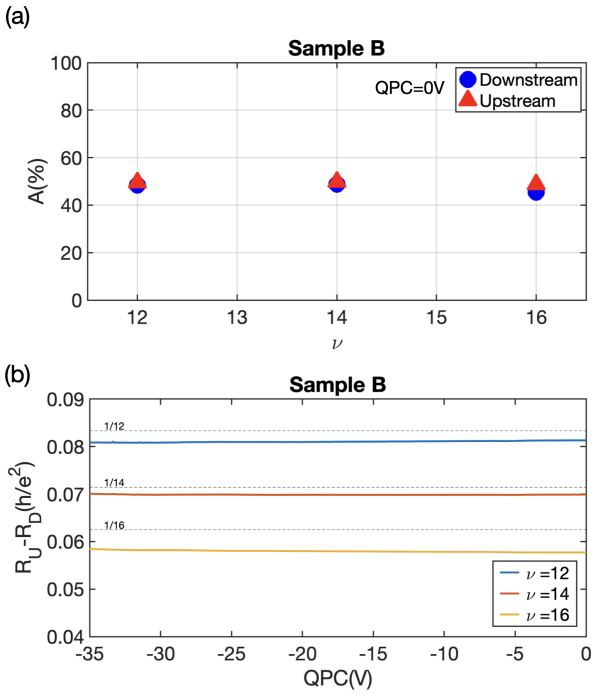

FIG. 2: (a) The extracted Andreev reflection data corresponds to three different filling factors: 12, 14, and 16. This data is obtained from both the R_U and R_D datasets at a QPC voltage of 0V. (b) The variation of the quantity $R_U - R_D$ is examined as a function of the QPC voltage.

We note that we are unable to extract from the experimental data A_s and ν_s independently from the above equations. But if we assume a fixed A_s, we notice (i) the value of R_U only depends on the number of edge modes passing through the QPC (ν_s); and (ii) the value of R_D depends on both the number of edge modes passing through the QPC and the bulk filling factor (ν).

* Electronic address: jshabani@nyu.edu

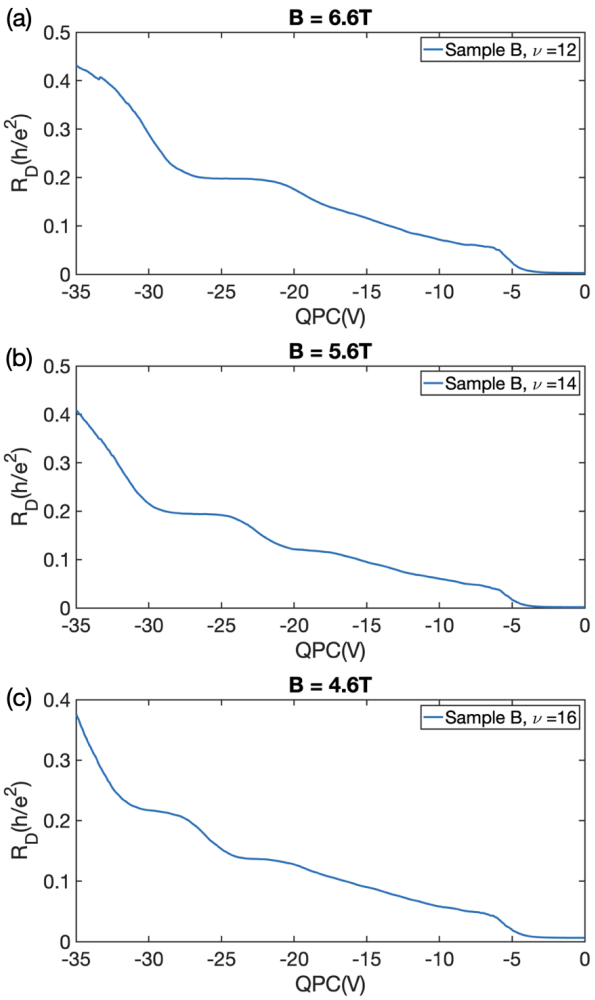

FIG. 3: The downstream resistance (R_D) is observed at various values of ν as a function of QPC voltage in three distinct cases: (a) $\nu = 12$, (b) $\nu = 14$, and (c) $\nu = 16$. The corresponding magnetic field for each filling factor is indicated above each panel.

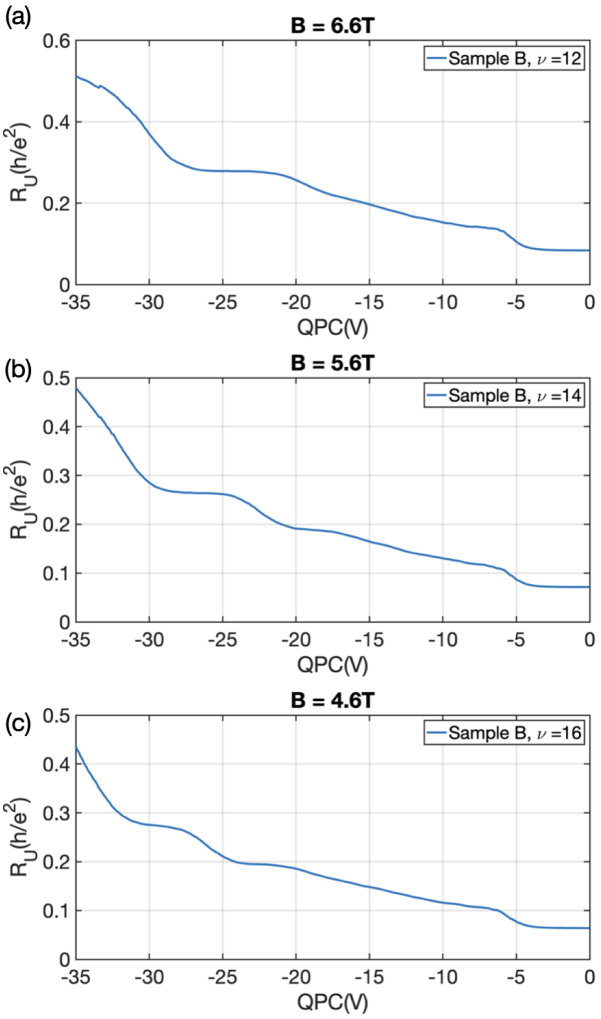

FIG. 4: The observed upstream resistance (R_U) is plotted against QPC voltage for various ν values: (a) 12, (b) 14, and (c) 16.

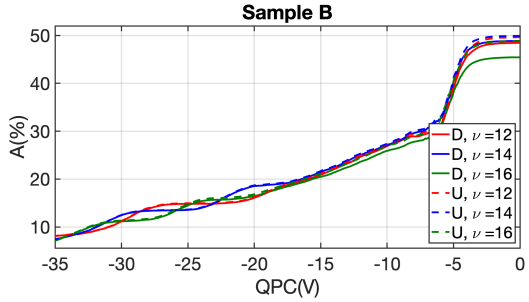

FIG. 5: The A parameter, derived from both upstream (U) and downstream (D) resistance, is presented as a function of QPC voltage for different filling factors ν.